Am J Transl Res 2025;17(7):5257-5270
www.ajtr.org /ISSN:1943-8141/AJTR0165034

Original Article

Spheroid culture of human periodontal ligament stem cells on agarose enhances stemness and osteogenic differentiation potential

Qinyao Zhang[1*], Shuwei Huang[1*], Jiumei Wu[1], Peng Liu[2], Jun Sun[3], Xing Xie[1], Mengjun Ge[3], Chuanmei Li[1], Mengyue Zhang[1], Lei Lei[1]

[1]Stem Cell and Regenerative Medicine Research Group, Xiangya School of Stomatology Central South University, Changsha 410000, Hunan, China; [2]College of Materials Science and Engineering, Hunan University, Changsha 410082, Hunan, China; [3]Department of Biomedical Sciences, College of Biology, Hunan University, Changsha 410082, Hunan, China. [*]Equal contributors and co-first authors.

Received April 3, 2025; Accepted June 24, 2025; Epub July 15, 2025; Published July 30, 2025

Abstract: Objective: To develop an agarose (AG)-based spheroid culture system to enhance the stemness and osteogenic potential of human periodontal ligament stem cells (hPDLSCs), addressing limitations of current periodontal tissue engineering approaches. Methods: hPDLSCs were isolated from extracted premolars and cultured as spheroids in AG-coated 96-well plates. Spheroid formation was optimized by varying cell seeding densities and culture durations. Monolayer-cultured hPDLSCs served as controls. Stemness was evaluated using RT-qPCR and immunofluorescence detection of pluripotency markers. Cell migratory capacity was assessed by scratch assays. Osteogenic differentiation was induced for 10-21 days, and calcium deposition was quantified by Alizarin Red S staining. Results: Spheroid-derived hPDLSCs showed significantly higher expression of stem cell markers (OCT4 and NANOG) and greater migratory capacity compared to monolayer-cultured cells. Upon osteogenic induction, spheroid-derived hPDLSCs exhibited upregulated expression of osteogenesis-related genes (BSP and OPN) and formed more extensive calcium nodules than their monolayer counterparts. Conclusion: The AG-based spheroid culture system effectively maintains hPDLSC stemness and enhances their osteogenic differentiation potential. This scalable and cost-effective platform provides high-quality seed cells for periodontal regeneration and holds promise for improving clinical outcomes in periodontal therapy.

Keywords: hPDLSC, agarose, cell spheroid, stemness, osteogenic differentiation

Introduction

Periodontitis is an inflammatory disease that damages the four key periodontal supporting tissues (gingiva, cementum, periodontal ligament, and alveolar bone) [1]. As the disease advances, it can cause tooth loosening, migration, and ultimately the loss of affected teeth [2]. Periodontitis is recognized as the sixth most prevalent chronic non-communicable disease globally, affecting approximately 10% of adults [3]. Its high prevalence imposes substantial social and economic burdens [4]. Conventional periodontal treatments primarily focus on controlling local inflammation. Although newer strategies - such as guided tissue regeneration, bone grafting, and local delivery of growth factors - have been developed, they still fall short of fully restoring the structure and function of damaged periodontal tissues [5].

To address this challenge, periodontal tissue engineering has emerged as a promising solution [6]. This approach combines seed cells, scaffolds, and growth factors to create an artificial regenerative microenvironment at the defect site. Among these, the seed cells are crucial, as they differentiate into the target cells needed to regenerate periodontal tissues. Human periodontal ligament stem cells (hPDLSCs) are the most extensively studied and rational seed cells for this purpose. However, obtaining a sufficient number of primary hPDLSCs remains challenging [7]. Although 2D culture

https://doi.org/10.62347/PPEI1766

techniques can expand hPDLSCs, they fail to replicate the native cellular processes and signaling pathways, leading to a loss of progenitor cell characteristics and reduced clinical efficacy [8].

In contrast, three-dimensional (3D) cell cultures enhance cell-cell and cell-extracellular matrix (ECM) interactions, better mimicking in vivo conditions [9]. 3D cultures help preserve and even enhance the original biological properties of cells, making them valuable tools for both basic research and translational applications [10]. Various methods have been explored to culture hPDLSCs in 3D, including hanging drop methods, cell sheets, conical tube pelleting, bioreactors, 3D printing, and low-adhesion techniques. In the hanging drop method, gravity promotes cell self-assembly, as cells accumulate at the tip of the droplet and spontaneously form spheroids [11]. However, these spheroids can quickly disperse, making long-term culture and scale-up difficult [12]. Cell sheets are generated by culturing cells to confluence, allowing them to form a dense endogenous ECM layer that can be detached. However, this method can damage cells and often yields variable results across batches [13]. In 2019, Iwasaki et al. cultured hPDLSCs in 15 mL polypropylene conical tubes and formed pellets by centrifugation at 180×g for five minutes, but the resulting cellular conditions were suboptimal [14]. Recently, bioreactor and 3D printing technologies have been applied for 3D culture of hPDLSCs; however, these methods require specialized and costly equipment [15, 16].

A traditional, biomimetic, and more cost-effective alternative is the use of low-adhesion surfaces to promote spontaneous cell aggregation. AG, extracted from red algae and composed of repeating units of D-galactose and 3, 6-anhydro-L-galactopyranose linked by alternating β-(1, 3) and β-(1, 4) glycosidic bonds [17], is widely used due to its thermo-reversible gelation properties [18]. When heated to 90-100°C, AG forms a clear solution as hydrogen bonds break; upon cooling to 30-40°C, hydrogen bonds reform, producing a tightly packed double-helix gel structure [17]. The hydrophilic and electrically neutral nature of AG prevents cell adhesion [19, 20], making it suitable for 3D cultures. Additionally, the curved AG surface in 96-well plates facilitate cell aggregation and accelerates spheroid formation [21]. Recent studies have confirmed that low-adhesion AG surfaces can induce spontaneous spheroid formation of mesenchymal stem cells (MSCs) without external stimuli [22, 23].

In this study, we aimed to develop a cost-effective and reproducible AG-based spheroid culture system to enhance the stemness and osteogenic differentiation potential of hPDLSCs. By optimizing spheroid formation conditions and characterizing the biological effects of this 3D culture method, we sought to establish a robust platform for producing high-quality hPDLSCs for periodontal tissue regeneration. This strategy holds promise for improving clinical outcomes in periodontal therapy and may have broader applications in regenerative medicine.

Materials and methods

Fabrication of AG low-adhesion plates

The process for fabricating AG low-adhesion plates is illustrated in **Figure 1A**. Specifically, 0.67 g of Dulbecco's Modified Eagle Medium (DMEM) powder (Gibco, USA) and 0.185 g of sodium bicarbonate (Sigma, USA) were dissolved in 25 mL of sterile water and prewarmed in a 37°C water bath. The solution was sterilized in a biosafety cabinet using a 0.22 μm filter membrane. Separately, 0.25 g of AG powder (Life Technologies, USA) was dissolved in 25 mL of sterile water and heated to boil in a microwave oven to ensure complete melting. The two solutions were then mixed in equal volumes. Next, 60 μL of the mixture was dispensed into each well of a 96-well plate positioned at a 45° angle inside a biosafety cabinet. The plates were then exposed to UV light for 2 hours to ensure sterilization. Upon cooling and solidification, the mixture formed a uniform low-adhesion surface.

Characterization of AG low-adhesion plates

The surface wettability of AG at different concentrations was assessed by measuring the water contact angle, as previously described [24]. AG samples were cast into rectangular pieces (10 mm × 10 mm) and mounted on glass slides to create flat surfaces. Four sample types were prepared for comparison: 0.5% (AG only), 0.25% (AG + DMEM), 0.5% (AG +

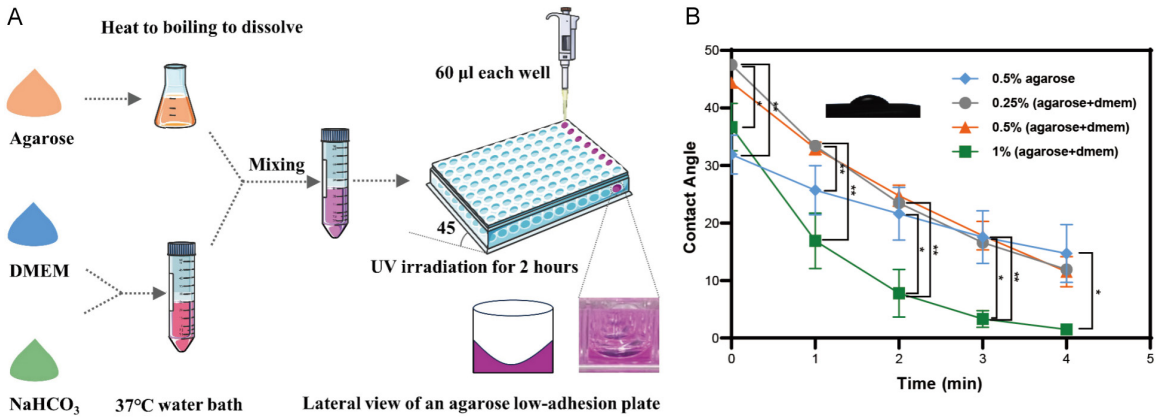

Figure 1. Fabrication and hydrophilicity characteristics of AG low adhesion plates. A. Procedure for the preparation of AG low adhesion plates. B. The hydrophilic properties of AG surfaces with different formulations at the same time point ($^{*}P < 0.05$, $^{**}P < 0.01$) (AG: agarose; DMEM: Dulbecco's Modified Eagle Medium).

DMEM), and 1% (AG + DMEM). Briefly, AG solutions were prepared by dissolving AG powder in sterile water to final concentrations of 0.25%, 0.5%, or 1% (w/v). Equal volumes of AG solution and DMEM solution were then mixed to produce AG + DMEM hydrogels. For contact angle measurement, a 2 μL droplet of deionized water was placed on each surface. Droplet images were captured every minute, and contact angles were recorded using a contact angle analyzer (SDC-200S, ShengDing, China).

The zeta potential of the AG low-adhesion surfaces was measured using a Nano ZS-90 Zetasizer (Malvern Instruments, UK). The crystal structure was characterized by X-ray diffraction (XRD, Miniflex600, Rigaku, Japan), and functional groups were identified by Fourier transform infrared spectroscopy (FTIR, Nicolet IS5, Thermo Scientific, USA).

Isolation and culture of hPDLSCs

This study was approved by the Medical Ethics Committee of Hunan Xiangya Stomatological Hospital, Central South University (approval number: 20220077). Written informed consent was obtained from all participants, and the study was conducted in accordance with the ethical standards of the 1964 Declaration of Helsinki. Premolar teeth extracted for orthodontic purposes were collected and rinsed five times with pre-cooled phosphate-buffered saline (PBS; Biosharp, China) containing 100 U/mL penicillin and 100 μg/mL streptomycin (Gibco, USA). Periodontal ligament tissue was gently scraped from the middle third of the root surface and then digested in a solution containing 3 mg/mL collagenase type I (Solarbio, China) and 4 mg/mL dispase II (Solarbio, China) mixed at a 1:1 ratio for 30 minutes at 37°C, with gentle agitation every five minutes.

After digestion, the tissue was transferred to 25 cm^2 culture flasks containing Mesenchymal Stem Cell Medium (MSCM; Sciencell, USA) and incubated at 37°C with 5% CO_2. The flasks were left undisturbed for the first four days. Fresh medium was added on day five, and thereafter the medium was changed every four days until cell colonies formed. When the hPDLSCs reached 70-80% confluence, they were dissociated using 0.25% trypsin (Gibco, USA). Cells were passaged every 2-3 days, and hPDLSCs at passages 3-6 were used for subsequent experiments.

Characterization of MSC surface markers and multilineage differentiation potential

To assess the expression of MSC surface markers, flow cytometry was performed. Briefly, 1 × 10^6 cells were dissociated with 0.25% trypsin and resuspended in PBS. The cell suspension was incubated with the following fluorochrome-conjugated anti-human antibodies: CD34-APC, CD45-PE, CD73-PE, and CD90-FITC. Samples were incubated in the dark at 4 C for 30 minutes, washed twice with PBS, and resuspended in 300 μL PBS for analysis using a flow cytometer. Data were analyzed using FlowJo software.

To verify multilineage differentiation potential, hPDLSCs were subjected to osteogenic, adipo-

Table 1. Primer sequences for real-time quantitative polymerase chain reaction (RT-qPCR)

Gene	Forward Primer Sequence (5'-3')	Reverse Primer Sequence (3'-5')
GAPDH	GAAGGTGAAGGTCGGAGTC	CTTTAGGGTAGTGGTAGAAG
OCT4	AGCAAAACCCGGAGGAGT	CTATATGTGTCCGGCTACACC
NANOG	CCCCAGCCTTTACTCTTCCTA	CCAGGTTGAATTGTTCCAGGTC
BSP	GAACCTCGTGGGGACAATTAC	CATCATAGCCATCGTAGCCTTG
OPN	GAAGTTTCGCAGACCTGACAT	GTATGCACCATTCAACTCCTCG

genic, and chondrogenic induction. For osteogenesis, cells were cultured for 21 days in medium containing 50 mg/L ascorbic acid, 10 mM β-glycerophosphate, and 100 nM dexamethasone, followed by Alizarin Red S staining to visualize calcium deposition. For adipogenesis, cells were cultured for 14 days in medium containing 1 μM dexamethasone, 0.5 mM 3-isobutyl-1-methylxanthine, and 200 μM indomethacin, and intracellular lipid droplets were stained with Oil Red O. For chondrogenesis, cells were cultured for 28 days in medium supplemented with 10 ng/mL TGF-β3, 50 μg/mL ascorbic acid, and 1% ITS Premix; sulfated glycosaminoglycans were detected using 1% Alcian Blue staining.

Spheroids formation

Passage 5 (P5) hPDLSCs were used for 3D spheroid formation. The cells were dissociated into a single-cell suspension using trypsin and seeded into 96-well plates at densities of 5,000, 10,000, or 50,000 cells per well. The cells were cultured at 37°C in a humidified incubator with 5% CO_2, with the plates inclined at a 45° angle. Notably, hPDLSCs spontaneously formed spheroids via self-aggregation. A half-volume medium change was performed on the second day. Morphology and diameter of the spheroids were observed and recorded using an inverted microscope (IX73, Olympus, Japan).

Cell viability assay

After carefully removing the medium, P5 hPDLSC spheroids were incubated with Calcein AM/propidium iodide working solution (Calcein AM/PI Cell Viability/Cytotoxicity Assay Kit, Beyotime, China) for 30 minutes. Stained samples were visualized and imaged using a fluorescence microscope (IX73, Olympus, Japan) to simultaneously detect live cells (green fluorescence) and dead cells (red fluorescence) within the spheroids.

Real-time quantitative polymerase chain reaction (RT-qPCR)

Total RNA was extracted using TRIzol reagent (Thermo Fisher Scientific, USA), and RNA concentration was determined with a Nanodrop 2000 spectrophotometer. Complementary DNA was synthesized using a PrimeScript RT kit (Perfect Real Time, Takara, Japan). RT-qPCR was performed with a Hieff qPCR SYBR Green Master Mix kit (Yeasen, China) under the following cycling conditions: 95°C for 10 minutes; 40 cycles of 95°C for 10 seconds, 55°C for 20 seconds, and 72°C for 20 seconds; followed by a final dissociation step. Gene-specific primer sequences are listed in **Table 1**. Expression levels of target genes were normalized to GAPDH and calculated using the 2^-ΔΔCT method.

Immunofluorescence staining

Spheroids and monolayer cells P5 were seeded into 96-well plates and cultured for 3 days. Cells were fixed with 4% paraformaldehyde for 20 minutes at room temperature and permeabilized with 0.1% Triton X-100 (Solarbio, China) for 10 min. After rinsing with PBS, cells were blocked with 5% fetal bovine serum and incubated overnight at 4°C with primary antibodies against Oct4 (Abcam, USA; 1:250) and Nanog (Abcam, USA; 1:250). After washing with PBS, cells were incubated with Alexa Fluor 488-conjugated goat anti-rabbit IgG secondary antibody (Abcam, USA; 1:500) for 2 hours at room temperature in the dark. Nuclei were counterstained with 4', 6-diamidino-2-phenylindole (DAPI; Biosharp, China) for 5 minutes. The stained samples were mounted with VECTASHIELD mounting medium and covered with a coverslip. Images were acquired using a fluorescence microscope (FV1200, Olympus, Japan).

Cell migration assay

A scratch wound healing assay was performed to evaluate the migration capacity of hPDLSCs derived from both spheroid and monolayer cul-

tures. Spheroids and monolayer cells P5 were dissociated with trypsin and seeded into sterile 6-well plates, allowing them to reach 95-100% confluence. A sterile P-200 pipette tip was used to create a scratch in each well. Images were captured at 0, 12, and 24 hours using a phase-contrast inverted microscope. Wound areas were analyzed with ImageJ software (National Institutes of Health, Bethesda, MD, USA). The relative migration rate (%) was calculated as: The relative migration rate (%) was calculated as [(Initial wound area - Wound area at time t)/ Initial wound area] × 100. Each group was evaluated in triplicate, and the entire experiment was repeated 3 times.

Osteogenic differentiation

Spheroids and monolayer cells were dissociated into single-cell suspensions and seeded in 6-well plates at a density of 1×10^5 cells per well. The following day, the medium was replaced with osteogenic induction medium (DMEM supplemented with 10% FBS, 50 mg/L vitamin C, 10 mM β-sodium glycerophosphate, and 10 nM dexamethasone). Cells were cultured in this medium for 10-21 days. After fixation with 4% paraformaldehyde for 30 min, cells were stained with Alizarin Red S (Solarbio, China) for 5 min at room temperature to detect calcium deposition. Calcium nodules were visualized using an inverted microscope (ECLIPSE TS100, Nikon, Japan). For quantification, the calcium deposits were dissolved with 10% cetylpyridinium chloride (Macklin, China) for 30 minutes, and the absorbance was measured at 562 nm.

Statistical analysis

All data are presented as mean ± standard deviation (SD) unless otherwise specified. Statistical comparisons between the two groups were performed using a two-tailed paired Student's t-test in GraphPad Prism 8.0.2 (GraphPad Software Inc., USA). A p-value < 0.05 was considered statistically significant, with *, **, ***, and **** indicating P < 0.05, P < 0.01, P < 0.001, and P < 0.0001, respectively.

Results

Fabrication and hydrophilicity characteristics of AG surfaces

The wettability of AG surfaces prepared at various concentrations was evaluated, as surface wettability is a prerequisite and critical parameter for cell-biomaterial interactions [25]. As shown in **Figure 1B**, the 0.5% AG alone and the 0.5% (AG + DMEM) groups exhibited distinct initial contact angles, with the 0.5% AG alone group showing a slightly more hydrophilic surface. However, the contact angles for both groups decreased over time and intersected at 3 minutes, indicating comparable hydrophilic properties. This suggests that the addition of DMEM to the AG gel did not significantly affect surface wettability. Additionally, no significant differences were observed between the 0.25% (AG + DMEM) and 0.5% (AG + DMEM) groups in both initial and late-phase (3-minute) contact angles (**Figure 1B**). In contrast, the 1% (AG + DMEM) group displayed the smallest initial and 3-minute contact angles, indicating the highest hydrophilicity.

Characteristics of hPDLSCs

Passage 3 hPDLSCs exhibited fibroblast-like morphologies (**Figure 2A**). Flow cytometry confirmed that the cells expressed MSC markers CD73 and CD90 (**Figure 2B**, **2C**), while hematopoietic markers CD34 and CD45 were not detected (**Figure 2D**, **2E**). After 21 days of osteogenic induction, extensive calcium deposition was observed, as evidenced by strong Alizarin Red S staining. Adipogenic differentiation resulted in intracellular lipid droplets stained with Oil Red O, while chondrogenic pellets developed a dense ECM rich in glycosaminoglycans, highlighted by Alcian Blue staining (**Figure 2F**). These results collectively demonstrate that the isolated cells meet the criteria defining MSCs.

Morphologies of characteristics of AG plates

The AG coatings on the plate wells appeared homogeneous and smooth when viewed from above, with no visible irregularities (**Figure 3A**). Side views revealed that the AG matrix formed a concave surface, with a smooth curvature extending from the well edges toward the center (**Figure 3B**). Upon seeding on these AG surfaces, hPDLSCs spontaneously aggregated into cell spheroids (**Figure 3C**, top view; **Figure 3D**, side view). Among the various formulations tested, the 1% (AG + DMEM) mixture did not support spheroid formation, whereas the other formulations did, with no significant differences in spheroid morphology observed (**Figure 3E**). Considering the enhanced mechanical strength and stability of higher AG concentrations - and the fact that a mechanically stronger substrate

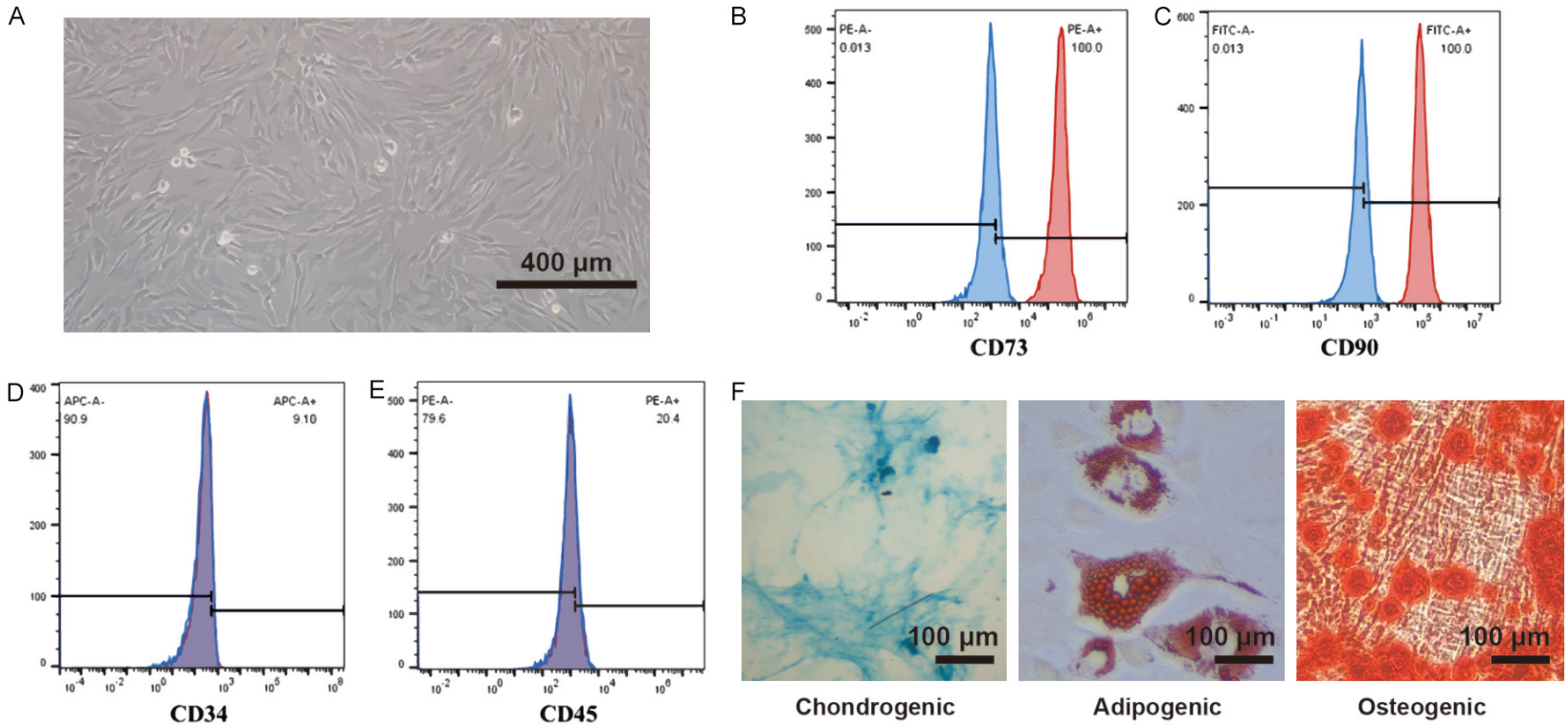

Figure 2. Characteristics of patient-derived hPDLSCs. A. Bright-field morphology of hPDLSCs. B-E. The expression patterns of CD73, CD90, CD34 and CD45. F. Alcian Blue staining of chondrogenic pellets, Oil Red O staining of adipogenic differentiation, Alizarin Red S staining of osteogenic differentiation.

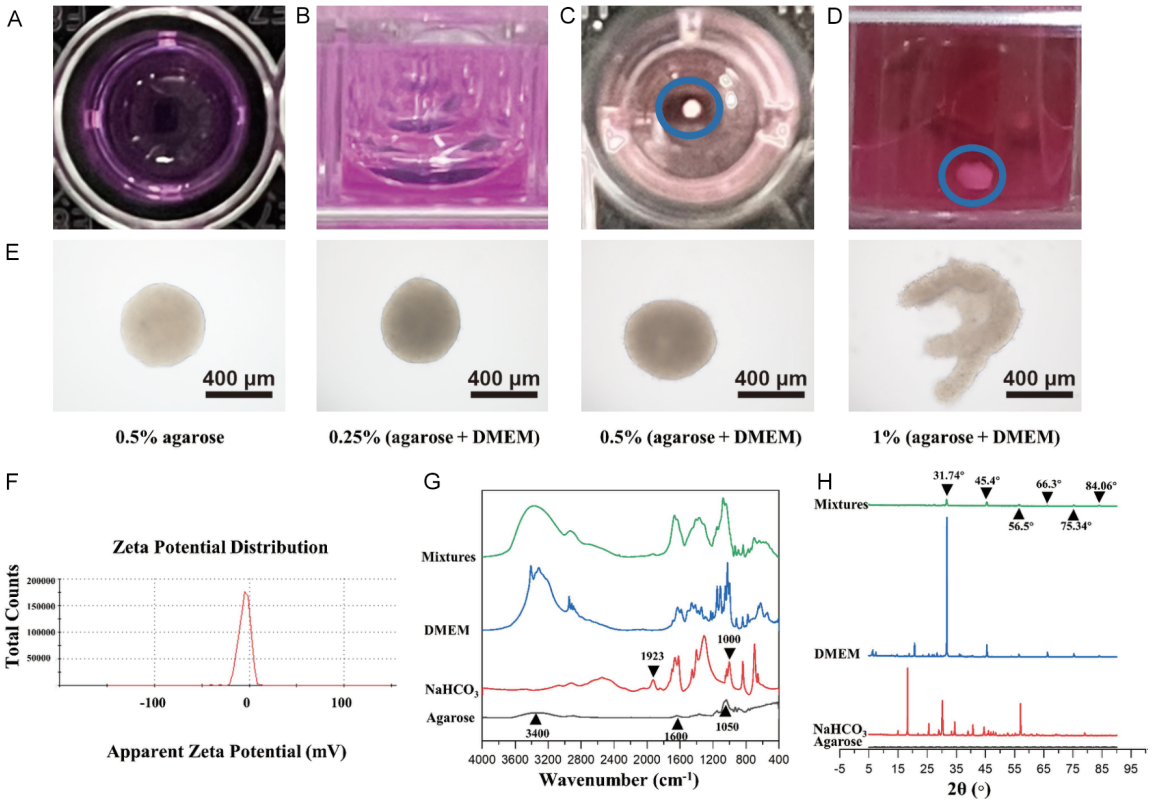

Figure 3. Morphologies of AG plates and the formed hPDLSC spheroids. A. Top view of an AG low-adhesion plate. B. Lateral view of an AG low-adhesion plate. C. Top view of spheroidal morphology of hPDLSCs. D. Lateral view of spheroidal morphology of hPDLSCs. E. 12-hour morphology of hPDLSCs cultured on different AG formulations. F. Zeta potential analysis of 0.5% (agarose + DMEM) plates. G. FTIR spectra of 0.5% (agarose + DMEM) plates. H. XRD patterns of 0.5% (agarose + DMEM) plates (DMEM: Dulbecco's Modified Eagle Medium).

can minimize external disturbances and maintain a stable experimental environment [17] - the 0.5% (AG + DMEM) formulation was selected for subsequent experiments.

The zeta potential of the 0.5% (AG + DMEM) surface was measured at -4.97 ± 5.89 mV (**Figure 3F**), indicating that the AG hydrogel is hydrophilic with a relatively negative surface charge, which may hinder hPDLSC adhesion. FTIR analysis confirmed that the coating was composed of biocompatible components - AG, sodium bicarbonate, and DMEM. AG displayed characteristic peaks near 1050 cm^{-1}, 1600 cm^{-1}, and 3400 cm^{-1}, corresponding to the stretching vibrations of C-O, O-H, N-H, and C = C bonds, respectively (**Figure 3G**) [26]. Sodium bicarbonate exhibited peaks near 1923 cm^{-1} and 1000 cm^{-1} (**Figure 3G**) [27]. These peaks were also detected in the mixture. Because DMEM is itself a complex mixture, it lacks a single distinctive FTIR peak; therefore, X-ray diffraction was performed to supplement the FTIR data. The diffraction patterns confirmed that the characteristic phase peaks of DMEM were preserved in the mixture (**Figure 3H**). No significant peak shifts were observed, indicating that the structural integrity of DMEM was maintained during fabrication. In summary, the hydrogel consisted solely of AG, sodium bicarbonate, and DMEM, with no chemical reactions occurring on the hydrophilic surface. This mixture effectively promoted hPDLSC spheroid formation.

Formation of hPDLSC spheroids

To investigate how initial cell number affects the morphology, diameter, and circularity of hPDLSC spheroids, 5,000, 10,000, and 50,000 cells were seeded onto 0.5% (AG + DMEM) surfaces and cultured for 5 days. As shown in **Figure 4A**, spheroid diameters decreased over time across all groups, indicating enhanced cell-cell interactions during spheroid maturation. The diameter declined notably within the first three days and then stabilized (**Figure 4B**). The initial cell number strongly influenced sp-

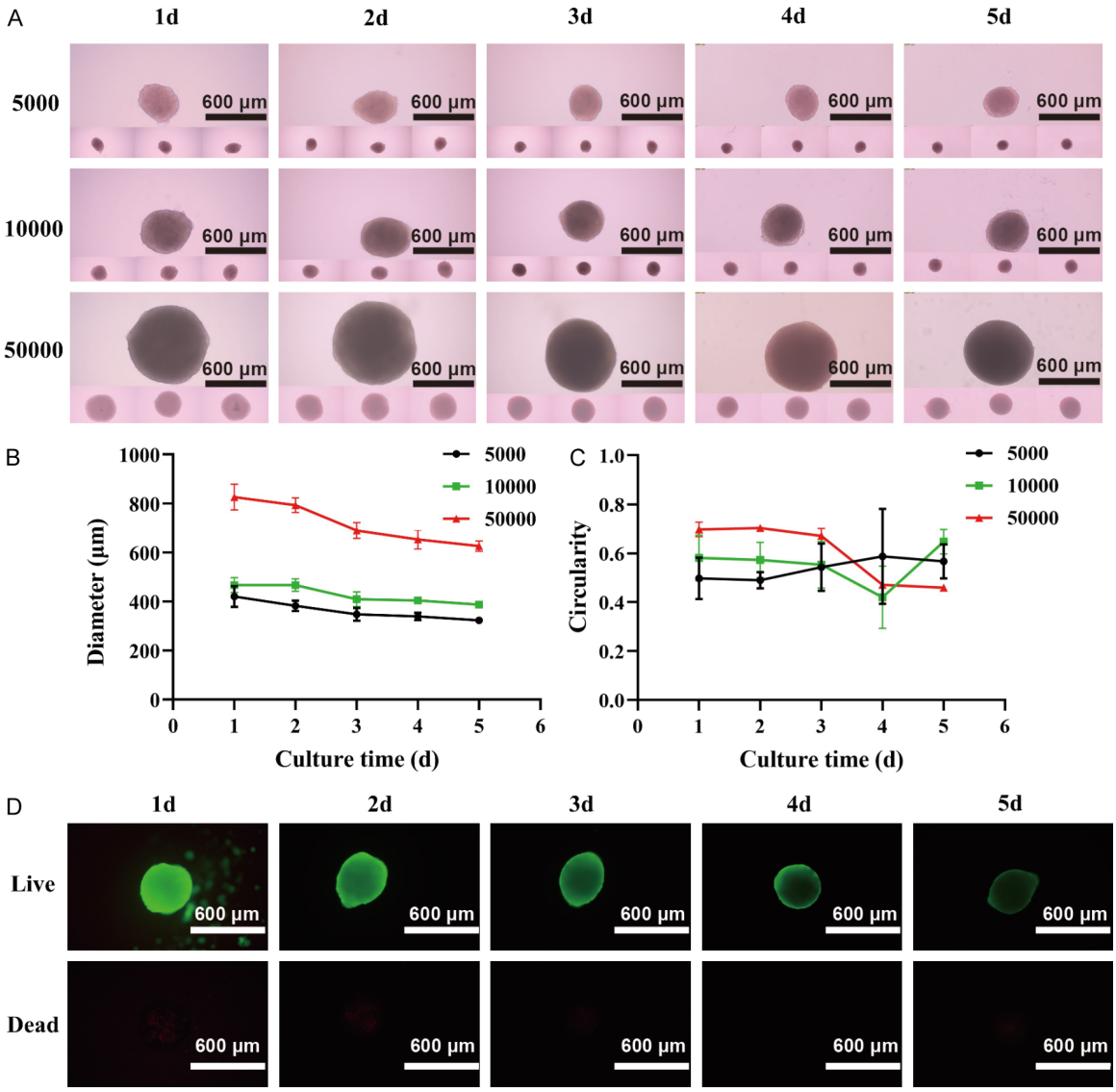

Figure 4. Formation of hPDLSC spheroids. A. Morphological changes of spheroids with cell numbers of 5,000, 10,000, and 50,000, respectively, over culture time. B. Changes in diameter of spheroids with cell numbers of 5,000, 10,000, 50,000 over culture time. C. Change in Circularity of spheroids with cell numbers of 5,000, 10,000, and 50,000 over culture time. D. Calcein AM/PI cell activity assay of hPDLSC spheroids over culture time. Live cells were stained green, and dead cells were stained red.

heroid size: spheroids formed from 5,000 cells measured 300-450 μm, those from 10,000 cells measured 350-450 μm, and those from 50,000 cells measured 600-800 μm (**Figure 4B**).

Circularity remained relatively stable from day 1 onward and was not significantly affected by the initial cell number (**Figure 4C**). Prior studies have shown that spheroid size affects MSC biological properties: smaller spheroids generally display greater resistance to senescence and higher differentiation potential [28]. Considering nutrient and oxygen supply limitations in larger spheroids, this study selected spheroids formed from 10,000 cells for subsequent assays to balance biological performance and ease of handling.

A live/dead assay confirmed that most cells within the spheroids remained viable after 5 days (**Figure 4D**). While spheroid size continued to decrease over time, the fluorescence intensity of Calcein AM also gradually diminished, consistent with observations from other 3D culture studies [29]. It is well known that cell death

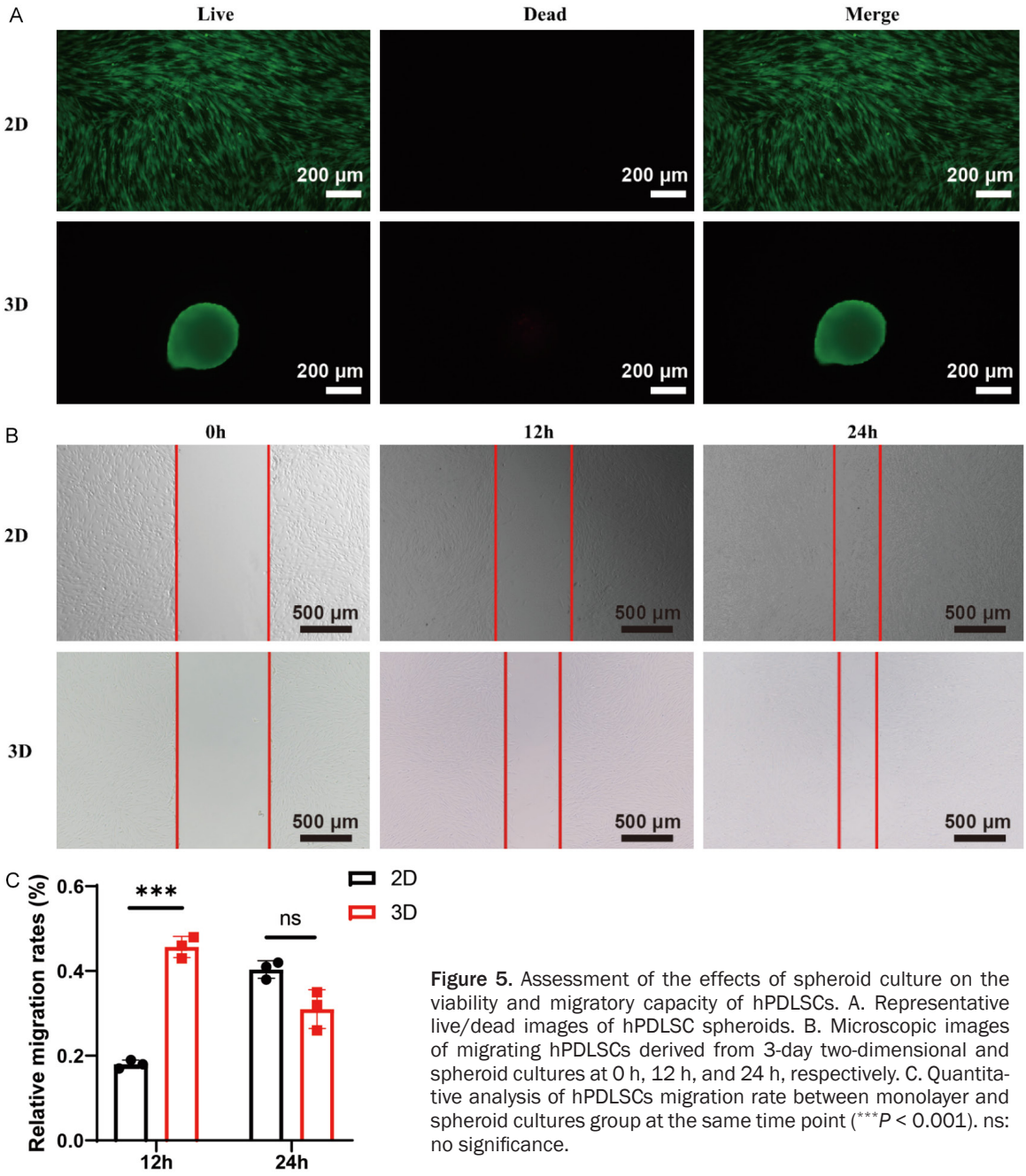

Figure 5. Assessment of the effects of spheroid culture on the viability and migratory capacity of hPDLSCs. A. Representative live/dead images of hPDLSC spheroids. B. Microscopic images of migrating hPDLSCs derived from 3-day two-dimensional and spheroid cultures at 0 h, 12 h, and 24 h, respectively. C. Quantitative analysis of hPDLSCs migration rate between monolayer and spheroid cultures group at the same time point (***$P < 0.001$). ns: no significance.

can occur in spheroid cores due to restricted nutrient diffusion, oxygen depletion, and metabolite accumulation [30, 31]. Based on these findings, 10,000 cells per spheroid and a 3-day culture period were selected for subsequent experiments.

Effect of spheroid culture on viability and migratory capacity of hPDLSCs

Cell viability in spheroids was further evaluated and compared to monolayer cultures using Calcein AM/PI staining. As shown in **Figure 5A**, monolayer-cultured hPDLSCs showed robust viability with minimal cell death, while spheroids exhibited only minor cell death at the spheroid core.

To assess the impact of spheroid culture on migratory ability, scratch wound healing assays were performed. The migration rates of spheroid-derived hPDLSCs were significantly higher than those of monolayer-derived cells at the same passage (**Figure 5B**, **5C**).

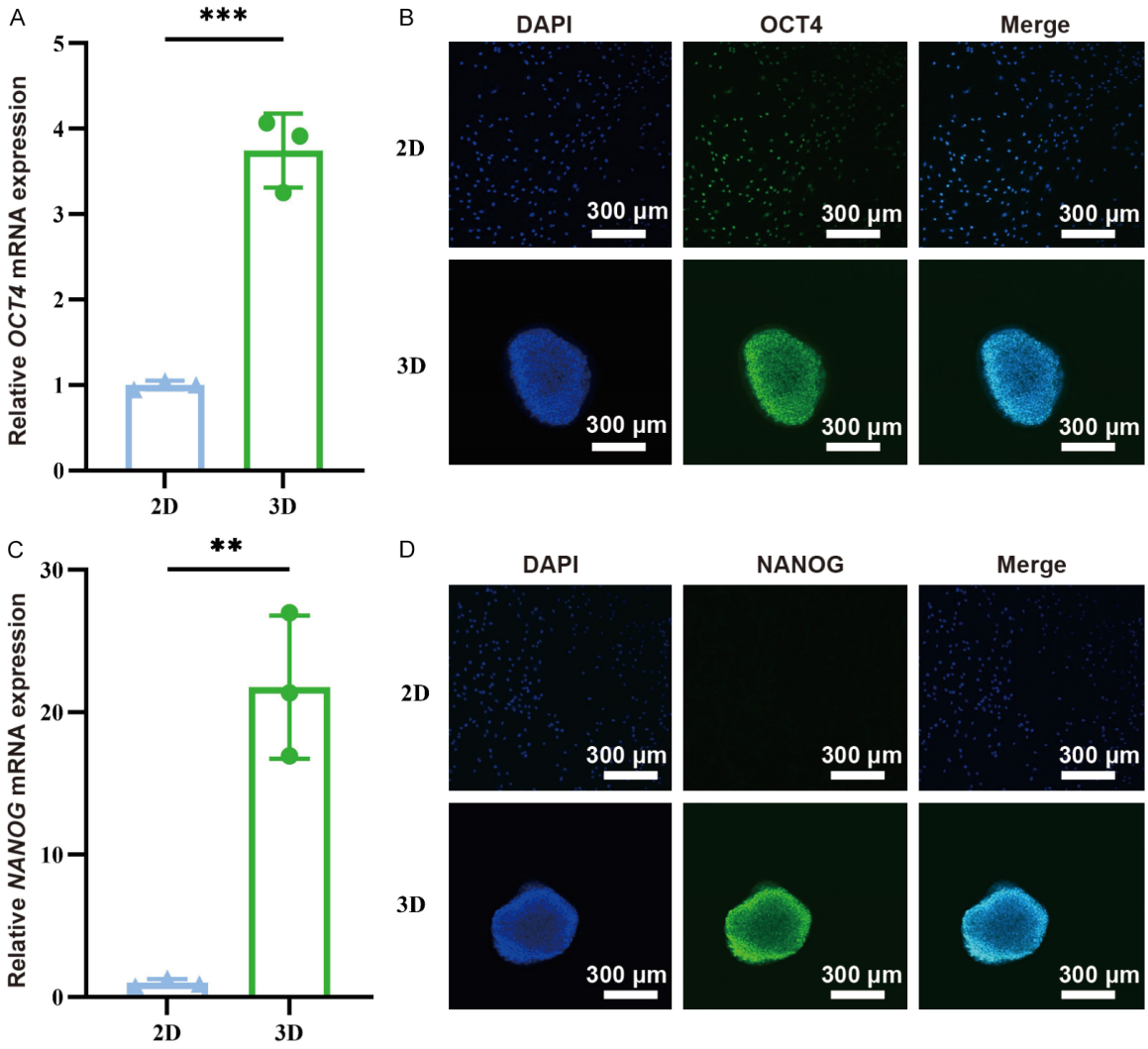

Figure 6. Enhancement of stemness of hPDLSC in cell spheroids. A. mRNA expression ofOCT4 in hPDLSCs from monolayers and spheroids (***$P < 0.001$). B. OCT4 protein expression in hPDLSCs in monolayer and spheroid cultures. C. mRNA expression of NANOG in hPDLSCs from monolayers and spheroids (**$P < 0.01$). D. NANOG protein expression in hPDLSCs in monolayer and spheroid cultures (DAPI: 4', 6-diamidino-2-phenylindole).

Enhancement of cell stemness in spheroids

hPDLSCs were cultured under monolayer and spheroid conditions for 3 days to evaluate stemness. RT-qPCR and immunofluorescence staining were conducted to compare the expression of stemness markers between groups. As shown in **Figure 6A**, **6C**, the mRNA levels of OCT4 and NANOG were significantly higher in spheroid-cultured cells than in monolayer cultures. At the protein level, monolayer hPDLSCs displayed weak OCT4 expression and undetectable NANOG expression (**Figure 6B**, **6D**). In contrast, spheroid-cultured cells exhibited robust expression of both markers. These findings indicate that spheroid culture significantly enhances the stemness of hPDLSCs compared to conventional monolayer culture.

Enhancement of osteogenic differentiation potential in spheroids

To investigate osteogenic potential, the expression of osteogenesis-related genes was analyzed by RT-qPCR after 10 days of osteogenic induction. The expression levels were significantly higher in spheroid-derived hPDLSCs compared to monolayer-derived cells (**Figure 7A**, **7B**). Alizarin Red S staining further confirmed enhanced mineral nodule formation in spheroid-derived cells (**Figure 7C**), and semi-

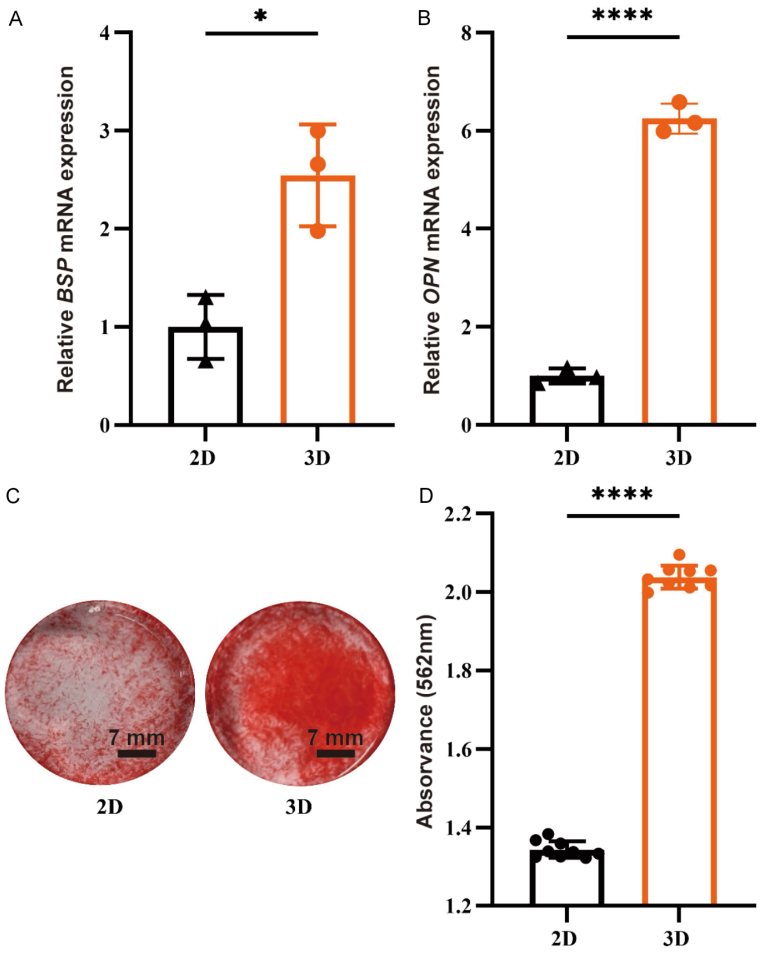

Figure 7. Enhancement of osteogenic differentiation potential of hPDLSCs derived from spheroids. A, B. mRNA expression of *BSP* and *OPN* in hPDLSCs from monolayers and spheroids after 10 days of osteogenic differentiation ($^{*}P < 0.05$, $^{****}P < 0.0001$). C. Alizarin Red S staining of calcium nodules after 21 days of osteogenic differentiation. D. Quantification of calcium of hPDLSCs from monolayers and spheroids after 21 days of osteogenic differentiation ($^{****}P < 0.0001$).

quantitative analysis of calcium content showed consistent results (**Figure 7D**). Notably, even after dissociation by trypsin, spheroid-derived hPDLSCs retained higher osteogenic differentiation capacity than monolayer-derived cells at the same passage, suggesting that spheroid culture not only enhances stemness but also sustains it over time.

Discussion

In 2006, Dominici et al. proposed minimum criteria for defining MSCs), including their ability to adhere to plastic surfaces, express specific markers (CD105, CD73, and CD90), and lack expression of hematopoietic markers (CD45, CD34, CD14, CD79a, or HLA-class II) [32]. Additionally, MSCs must be capable of differentiating into osteogenic, adipogenic, and chondrogenic lineages in vitro. The periodontal ligament-derived cells used in this study exhibited morphological characteristics consistent with previously reported hPDLSCs [33] and satisfied established criteria.

Currently, spheroid culture models are broadly categorized as scaffold-based or scaffold-free. Scaffold-based models rely on selecting appropriate scaffolds tailored to the target cell type [34]. These scaffolds mimic the ECM, promoting cell-cell and cell-ECM interactions and signaling. By contrast, scaffold-free approaches - including low-adhesion culture plates, hanging drop cultures, and rotating bioreactors - enable cells to self-aggregate into spheroids while preserving their native properties [11-14, 34]. In this study, considering factors such as cost-effectiveness, mechanical stability, environmental sustainability, and biocompatibility, we employed AG-coated 96-well plates combined with an inclined culture setup to create a low-adhesion, hydrophilic surface that promotes the spontaneous aggregation of hPDLSCs into spheroids.

Our spheroid culture system used well-defined components - AG, sodium bicarbonate, and DMEM - though slight concentration variations may occur during preparation. To ensure material purity and consistency, we validated the composition using FTIR and XRD analyses, enhancing the reproducibility and reliability of our results. Additionally, because material mixtures can affect physicochemical properties, we measured the zeta potential to characterize surface charge. These steps collectively ensured experimental consistency, which is vital for studying spheroid effects on hPDLSC behav-

ior, including adhesion, proliferation, and differentiation.

The biological properties of hPDLSCs - particularly cell viability and migration - are critical for effective periodontal regeneration. Our results demonstrated that spheroid-cultured hPDLSCs exhibited superior migration ability compared to monolayer-cultured cells, consistent with previous studies [35]. Within spheroids, gradients of oxygen and nutrients form: the outer layer has high oxygen and proliferation rates, the middle zone contains quiescent cells, and the core often becomes hypoxic, leading to necrosis and apoptosis [36]. Spheroid size critically influences these gradients and, consequently, cell survival. However, hypoxia is not entirely detrimental; in fact, low oxygen levels (2%) can enhance the expression of stemness markers such as SOX2, OCT4, and c-Myc, and increase the multipotency of dental-derived stem cells [37]. Our findings showed a direct correlation between initial cell number and spheroid diameter, aligning with previous reports [28, 29]. Moreover, spheroids formed with a given cell number showed minimal diameter changes over time, suggesting stable cell-cell interactions once aggregation occurs. This stability likely results from rapid ECM formation within the spheroid core, which limits further compaction. Accordingly, we optimized the spheroid diameter to approximately 300 μm to balance ECM-mediated structural integrity and minimize central necrosis due to limited nutrient and oxygen diffusion. This optimization supports both enhanced stemness and improved migration while mitigating hypoxia-induced apoptosis.

OCT4 and NANOG are well-established transcription factors that indicate stemness and pluripotency in MSCs [38]. This study confirmed that spheroid-cultured hPDLSCs exhibited significantly higher OCT4 and NANOG expression at both mRNA and protein levels compared to monolayer cultures, corroborating reports that spheroid systems enhance stemness [39, 40]. However, discrepancies exist in the literature regarding spheroid effects on hPDLSC stemness [14], possibly due to differences in spheroid formation methods. Importantly, our study did not explore the precise mechanisms by which spheroid culture maintains stemness in vitro - a limitation that should be addressed in future research.

We further evaluated the osteogenic differentiation capacity of spheroid-derived versus monolayer-derived hPDLSCs. Given that hPDLSCs originate from the periodontium, their osteogenic potential holds particular clinical relevance. Our findings showed that spheroid-derived hPDLSCs exhibited markedly enhanced osteogenic differentiation at both genetic and cellular levels, in line with previous studies highlighting the osteo-inductive advantage of spheroid culture [41]. A limitation of this work is the lack of in vivo validation, which will be critical for confirming the translational potential of these findings.

In summary, we developed a spheroid culture system that enhances the stemness and osteogenic differentiation of hPDLSCs compared to conventional monolayer cultures. By seeding 10,000 cells per well onto a 0.5% (AG + DMEM) hydrogel and culturing for 3 days, we generated robust, viable spheroids. Evaluations of cell viability, stemness markers, migration capacity, and osteogenic differentiation confirmed that spheroid culture confers significant advantages over monolayer culture. While slight reductions in viability within spheroids were observed, the overall gains in stemness and osteogenic potential outweigh this minor drawback.

In conclusion, this study presents an AG-based spheroid culture method for hPDLSCs. The 0.5% (AG + DMEM) hydrogel surface effectively induces the formation of hPDLSC spheroids that retain higher stemness and osteogenic differentiation capacity than cells maintained in monolayer culture. These spheroid-derived hPDLSCs hold promise for advancing clinical strategies to repair and regenerate periodontal tissues.

Acknowledgements

This work was supported by the Postgraduate Scientific Research Innovation Project of Hunan Province (Nos. CX20220353, CX20230367) and Postgraduate Scientific Research Innovation Project of Central South University (No. 1053320222830, No. 1053320232218).

Disclosure of conflict of interest

None.

Address correspondence to: Dr. Lei Lei, Stem Cell and Regenerative Medicine Research Group, Xiangya School of Stomatology Central South University,

Changsha 410000, Hunan, China. Tel: +86-13874-931910; E-mail: leilei8413@csu.edu.cn

References

[1] Hajishengallis G. Interconnection of periodontal disease and comorbidities: evidence, mechanisms, and implications. Periodontol 2000 2022; 89: 9-18.

[2] Agnese CCD, Schöffer C, Kantorski KZ, Zanatta FB, Susin C and Antoniazzi RP. Periodontitis and oral health-related quality of life: a systematic review and meta-analysis. J Clin Periodontol 2025; 52: 408-420.

[3] Trindade D, Carvalho R, Machado V, Chambrone L, Mendes JJ and Botelho J. Prevalence of periodontitis in dentate people between 2011 and 2020: a systematic review and meta-analysis of epidemiological studies. J Clin Periodontol 2023; 50: 604-626.

[4] Cui Y, Tian G, Li R, Shi Y, Zhou T and Yan Y. Epidemiological and sociodemographic transitions of severe periodontitis incidence, prevalence, and disability-adjusted life years for 21 world regions and globally from 1990 to 2019: an age-period-cohort analysis. J Periodontol 2023; 94: 193-203.

[5] Bartold PM, McCulloch CA, Narayanan AS and Pitaru S. Tissue engineering: a new paradigm for periodontal regeneration based on molecular and cell biology. Periodontol 2000 2000; 24: 253-269.

[6] Liu Y, Guo L, Li X, Liu S, Du J, Xu J, Hu J and Liu Y. Challenges and tissue engineering strategies of periodontal-guided tissue regeneration. Tissue Eng Part C Methods 2022; 28: 405-419.

[7] Chen FM and Jin Y. Periodontal tissue engineering and regeneration: current approaches and expanding opportunities. Tissue Eng Part B Rev 2010; 16: 219-255.

[8] Huang J, Zhang L, Lu A and Liang C. Organoids as innovative models for bone and joint diseases. Cells 2023; 12: 1590.

[9] Wu X, Su J, Wei J, Jiang N and Ge X. Recent advances in three-dimensional stem cell culture systems and applications. Stem Cells Int 2021; 2021: 9477332.

[10] Krasnova O, Kovaleva A, Saveleva A, Kulakova K, Bystrova O, Martynova M, Domnina A, Sopova J and Neganova I. Mesenchymal stem cells lose the senescent phenotype under 3D cultivation. Stem Cell Res Ther 2023; 14: 373.

[11] Sumbalova Koledova Z. 3D cell culture: techniques for and beyond organoid applications. Methods Mol Biol 2024; 2764: 1-12.

[12] Tevlek A, Kecili S, Ozcelik OS, Kulah H and Tekin HC. Spheroid engineering in microfluidic devices. ACS Omega 2023; 8: 3630-3649.

[13] Hu D, Li X, Li J, Tong P, Li Z, Lin G, Sun Y and Wang J. The preclinical and clinical progress of cell sheet engineering in regenerative medicine. Stem Cell Res Ther 2023; 14: 112.

[14] Iwasaki K, Nagata M, Akazawa K, Watabe T and Morita I. Changes in characteristics of periodontal ligament stem cells in spheroid culture. J Periodontal Res 2019; 54: 364-373.

[15] Mirsky NA, Ehlen QT, Greenfield JA, Antonietti M, Slavin BV, Nayak VV, Pelaez D, Tse DT, Witek L, Daunert S and Coelho PG. Three-dimensional bioprinting: a comprehensive review for applications in tissue engineering and regenerative medicine. Bioengineering (Basel) 2024; 11: 777.

[16] Ryu NE, Lee SH and Park H. Spheroid culture system methods and applications for mesenchymal stem cells. Cells 2019; 8: 1620.

[17] Jiang F, Xu XW, Chen FQ, Weng HF, Chen J, Ru Y, Xiao Q and Xiao AF. Extraction, modification and biomedical application of agarose hydrogels: a review. Mar Drugs 2023; 21: 299.

[18] Rotjanasuworapong K, Thummarungsan N, Lerdwijitjarud W and Sirivat A. Facile formation of agarose hydrogel and electromechanical responses as electro-responsive hydrogel materials in actuator applications. Carbohydr Polym 2020; 247: 116709.

[19] Ferrari M, Cirisano F and Morán MC. Mammalian cell spheroids on mixed organic-inorganic superhydrophobic coating. Molecules 2022; 27: 1247.

[20] Rasmussen K and Ostgaard K. Adhesion of the marine bacterium pseudomonas sp. NCIMB 2021 to different hydrogel surfaces. Water Res 2003; 37: 519-524.

[21] Fatimi A, Okoro OV, Podstawczyk D, Siminska-Stanny J and Shavandi A. Natural hydrogel-based bio-inks for 3D Bioprinting in tissue engineering: a review. Gels 2022; 8: 179.

[22] Mohebichamkhorami F, Niknam Z, Khoramjouy M, Heidarli E, Ghasemi R, Hosseinzadeh S, Mohseni SS, Hajikarim-Hamedani A, Heidari A, Ghane Y, Mahmoudifard M, Zali H and Faizi M. Brain homogenate of a rat model of alzheimer's disease modifies the secretome of 3d cultured periodontal ligament stem cells: a potential neuroregenerative therapy. Iran J Pharm Res 2022; 21: e133668.

[23] Silva-Carvalho AÉ, da Silva IGM, Corrêa JR and Saldanha-Araujo F. Regulatory T-Cell enhancement, expression of adhesion molecules, and production of anti-inflammatory factors are differentially modulated by spheroid-cultured mesenchymal stem cells. Int J Mol Sci 2022; 23: 14349.

[24] Liu P, Qiu T, Liu J, Long X, Wang X, Nie H, Yu M, Ma C, Lin N, Teoh SH and Wang Z. Mechanically enhanced and osteobioactive synthetic periosteum via development of poly(ε-capro-

lactone)/microtantalum composite. Colloids Surf B Biointerfaces 2023; 231: 113537.
[25] Spriano S, Sarath Chandra V, Cochis A, Uberti F, Rimondini L, Bertone E, Vitale A, Scolaro C, Ferrari M, Cirisano F, Gautier di Confiengo G and Ferraris S. How do wettability, zeta potential and hydroxylation degree affect the biological response of biomaterials? Mater Sci Eng C Mater Biol Appl 2017; 74: 542-555.
[26] Ali NI, Abidin SZZ, Majid SR and Jaafar NK. Role of Mg(NO(3))(2) as defective agent in ameliorating the electrical conductivity, structural and electrochemical properties of agarose-based polymer electrolytes. Polymers (Basel) 2021; 13: 3357.
[27] Joshi S, Kalyanasundaram S and Balasubramanian V. Quantitative analysis of sodium carbonate and sodium bicarbonate in solid mixtures using Fourier transform infrared spectroscopy (FT-IR). Appl Spectrosc 2013; 67: 841-845.
[28] Morsczeck C, Götz W, Schierholz J, Zeilhofer F, Kühn U, Möhl C, Sippel C and Hoffmann KH. Isolation of precursor cells (PCs) from human dental follicle of wisdom teeth. Matrix Biol 2005; 24: 155-165.
[29] Rolver MG, Elingaard-Larsen LO and Pedersen SF. Assessing cell viability and death in 3D spheroid cultures of cancer cells. J Vis Exp 2019.
[30] Wolff A, Frank M, Staehlke S and Peters K. A comparative study on the adipogenic differentiation of mesenchymal stem/stromal cells in 2D and 3D culture. Cells 2022; 11: 1313.
[31] Tsai AC, Liu Y, Yuan X and Ma T. Compaction, fusion, and functional activation of three-dimensional human mesenchymal stem cell aggregate. Tissue Eng Part A 2015; 21: 1705-1719.
[32] Dominici M, Le Blanc K, Mueller I, Slaper-Cortenbach I, Marini F, Krause D, Deans R, Keating A, Prockop D and Horwitz E. Minimal criteria for defining multipotent mesenchymal stromal cells. The International Society for Cellular Therapy position statement. Cytotherapy 2006; 8: 315-317.
[33] Yang Y, Alves T, Miao MZ, Wu YC, Li G, Lou J, Hasturk H, Van Dyke TE, Kantarci A and Wu D. Single-cell transcriptomic analysis of dental pulp and periodontal ligament stem cells. J Dent Res 2024; 103: 71-80.
[34] Pohlit H, Bohlin J, Katiyar N, Hilborn J and Tenje M. Technology platform for facile handling of 3D hydrogel cell culture scaffolds. Sci Rep 2023; 13: 12829.
[35] Yan Z, Yin H, Wu J, Tian G, Li M, Liao Z, He S, Deng H, Ning C, Ding Z, Yuan X, Sui X, Chen M, Liu S and Guo Q. Engineering exosomes by three-dimensional porous scaffold culture of human umbilical cord mesenchymal stem cells promote osteochondral repair. Mater Today Bio 2023; 19: 100549.
[36] Murphy KC, Hung BP, Browne-Bourne S, Zhou D, Yeung J, Genetos DC and Leach JK. Measurement of oxygen tension within mesenchymal stem cell spheroids. J R Soc Interface 2017; 14: 20160851.
[37] Samal JRK, Rangasami VK, Samanta S, Varghese OP and Oommen OP. Discrepancies on the role of oxygen gradient and culture condition on mesenchymal stem cell fate. Adv Healthc Mater 2021; 10: e2002058.
[38] Ali HRW, Suliman S, Osman TA, Carrasco M, Bruland O, Costea DE, Ræder H and Mustafa K. Xeno-free generation of human induced pluripotent stem cells from donor-matched fibroblasts isolated from dermal and oral tissues. Stem Cell Res Ther 2023; 14: 199.
[39] Kida K, Kanaki T, Gao S, Hatanaka D, Iwakami M, Liu S, Horikawa M, Ono M and Chang D. A novel 3D culture system using a chitin-based polysaccharide material produces high-quality allogeneic human UCMSCs with dispersed sphere morphology. Cells 2022; 11: 995.
[40] Chan YH, Lee YC, Hung CY, Yang PJ, Lai PC and Feng SW. Three-dimensional Spheroid culture enhances multipotent differentiation and stemness capacities of human dental pulp-derived mesenchymal stem cells by modulating MAPK and NF-kB signaling pathways. Stem Cell Rev Rep 2021; 17: 1810-1826.
[41] Li N, Dai X, Yang F, Sun Y, Wu X, Zhou Q, Chen K, Sun J, Bi W, Shi L and Yu Y. Spontaneous spheroids from alveolar bone-derived mesenchymal stromal cells maintain pluripotency of stem cells by regulating hypoxia-inducible factors. Biol Res 2023; 56: 17.